

Full length article

Influence of Ca adsorption on the heterogeneous nucleation of α -Mg on Al_4C_3 particles: First-principles calculation and experiment



Shu-Qing Yang^a, Cheng-Bo Li^a, Jun Du^{a,*}, Yu-Jun Zhao^{b,c,**}

^a School of Materials Science and Engineering, South China University of Technology, Guangzhou 510640, China

^b Department of Physics, South China University of Technology, Guangzhou 510640, China

^c Key Laboratory of Advanced Energy Storage Materials of Guangdong Province, South China University of Technology, Guangzhou 510640, China

ARTICLE INFO

Keywords:

Grain refinement

Heterogeneous nucleation

Al_4C_3

Surface adsorption

First-principles calculation

ABSTRACT

The addition of Ca in magnesium melt has a significant influence on the heterogeneous nucleation effect of Al_4C_3 particles with open question for the mechanism. We have conducted first-principles calculations of the adsorption of Ca and Mg atoms on Al_4C_3 surfaces to study the initial nucleation and growth of Mg atoms on Al_4C_3 surfaces. The single Ca or Mg adsorption, as well as Ca–Mg co-adsorption on a 28-layer slab (A-type) of Al-terminated $\text{Al}_4\text{C}_3(0001)$ surface has been simulated. We demonstrate that both Ca and Mg atoms tend to stabilize at the H2 site of Al-terminated $\text{Al}_4\text{C}_3(0001)$ surface. Meanwhile, a comparative experiment is conducted to study the influence of Ca on the grain refining effect, showing that Ca atoms promotes the adsorption and nucleation growth of Mg atoms on Al_4C_3 surfaces.

1. Introduction

Magnesium alloys have wide application prospects in aerospace and automotive components, 3C products, biomedical implants and other fields because of their excellent properties [1,2]. However, wider applications of Mg alloys are limited due to some disadvantages, such as low strength, low corrosion resistance, poor plasticity and toughness [3]. Many researchers have focused on the properties of Mg alloys for a long time and developed various approaches: grain refinement, work hardening, and strengthening with addition of alloy elements, etc. [3,4]. Grain refinement is an effective route to improve the comprehensive mechanical properties of Mg alloys [5]. Among the studies on grain refinement of Mg alloys, carbon inoculation has been considered as the most promising refinement method [3,6]. The viewpoint that Al_4C_3 particles formed in the carbon-inoculated Mg–Al melt act as potent nuclei of α -Mg grains has been widely recognized as the nucleation refining mechanism [7–9].

According to the theory of lattice registry [10–12], the interface misfit between the heterogeneous nucleus and matrix is a dominant factor to determine the nucleating potency. The heterogeneous nuclei will be more effective if the interface misfit is smaller. Moreover, the interfacial energy of nuclei/matrix interface is also a significant factor to determine the grain refining efficiency. However, it is hard to obtain

the interfacial energy based on experimental methods and analytical methods. During the past two decades, the first-principles calculation has been proved to be competent in various systems and widely used to evaluate the interface characteristics [13–15]. It has been used to analyze the grain refining mechanisms of steel [16,17], aluminum alloys [18,19] and Mg alloys [13,20–22]. Li et al. [20] and Wang et al. [21] calculated the interfacial energies of $\text{Al}_4\text{C}_3/\text{Mg}$ and $\text{Al}_2\text{MgC}_2/\text{Mg}$ interfaces, respectively. Both Al_4C_3 and Al_2MgC_2 should be potent nuclei of α -Mg grains since their interfacial energies are smaller than the interfacial energy of α -Mg/Mg melt. Moreover, Shin et al. [13] pointed out that the first-principles calculation was a useful tool for the research and development of new Mg alloys.

Many studies suggested that alloy elements often play an important role in the grain refinement of Mg alloys, such as Fe, Mn, Ca, Sr, Ce, Al, Si, and Zr [23–30]. During solidification, solute elements enrich in front of the solid/liquid interface due to re-distribution. Constitutional undercooling is induced, facilitating more heterogeneous particles activated to be potential nucleation substrates. In addition, the enrichment of solute elements in front of the solid/liquid interface reduces the diffusion rate of atom in the melt, inhibiting the grain growth. Consequently, grain refinement can be obtained due to more potent nuclei and grain growth inhibition. Moreover, some elements can disturb the nucleating potency by reaction with nuclei or adsorbed on the surfaces

* Correspondence to: J. Du, Department of Metallic Materials, School of Materials Science and Engineering, South China University of Technology, 381 Wushan Rd, Guangzhou, Guangdong 510640, China.

** Correspondence to: Y.-J. Zhao, Department of Physics, South China University of Technology, 381 Wushan Rd, Guangzhou, Guangdong 510640, China.

E-mail addresses: tandujun@sina.com (J. Du), zhaoyj@scut.edu.cn (Y.-J. Zhao).

<https://doi.org/10.1016/j.apsusc.2019.06.140>

Received 12 March 2019; Received in revised form 4 June 2019; Accepted 13 June 2019

Available online 14 June 2019

0169-4332/ © 2019 Published by Elsevier B.V.

of nuclei. Specially, adsorption of solute elements can change the surface characteristics of nuclei, resulting in the change of nucleating potency. Yao et al. [31] and Wei et al. [32] studied the adsorption of Mn and Fe on $\text{Al}_4\text{C}_3(0001)$ surface by the first-principles calculation, respectively. The adsorbed Mn and Fe atoms changed the surface configuration of $\text{Al}_4\text{C}_3(0001)$ -slab, which in turn affected the heterogeneous nucleation of Al_4C_3 particles.

An adsorption model of the heterogeneous nucleation of solidification was developed by Cantor et al. [33,34], who pointed out the importance of the atom adsorption on nucleating particle in the initial stage of heterogeneous nucleation process. Atom adsorption will influence the stability of nuclei and subsequent grain growth process. As for the carbon-inoculated Mg melt, the Mg atoms adsorb on the surface of Al_4C_3 in the initial stage solidification, followed by growth of stable Mg-adsorbed nuclei. In our previous study, a synergistic grain refining effect was found for Mg-3%Al refined by carbon inoculation combining Ca addition [23,35]. Better refining effect could be achieved due to the synergistic effect of Al_4C_3 heterogeneous nucleation and Ca element [23,35]. However, the influence mechanism of Ca has not been well understood.

Ca is a typical surface active element and it is apt to segregate ahead of S/L interface [36,37], thus it will adsorb on the Al_4C_3 surface and influence the adsorption of Mg atoms on the Al_4C_3 surface during the solidification progress. Limited by experimental and analytical methods, it is difficult to further analyze the influence mechanism of Ca on the adsorption and growth of Mg atoms on the surface of Al_4C_3 nuclei. In the present study, first-principles calculation was used to evaluate the surface characteristics of Al_4C_3 that adsorbed Ca or Mg atoms. The adsorption energy and electronic properties of Ca/Mg adsorption on the surface of Al_4C_3 were studied. The promotion mechanism of Ca on grain refinement of Mg–Al alloy induced by carbon inoculation was further analyzed.

2. Experimental results

Mg-3%Al (mass ratio, the same below) alloy was chosen as experimental material. Three series of experiments were conducted to investigate the influence of Ca in our study, i.e., Mg-3%Al alloy without any treatment, Mg-3%Al alloy treated with 0.2 wt.% C addition (carbon inoculation), and Mg-3%Al alloy treated with 0.2 wt.% C + 0.2 wt.% Ca addition (carbon inoculation combining with Ca addition). Graphite was used as carbon carbonaceous agent to inoculate Mg-3%Al melt. Addition contents of graphite and Ca were both 0.2% of the melt weight. The preparation details of the samples can be known in references [38]. Microstructure observation samples were prepared by standard metallographic techniques. The grain microstructures were observed by Leica DFC320 optical microscope. The carbon-rich nucleation particles were observed by electron probe microanalyzer (EPMA-1600) equipped with wave dispersive spectroscopy (WDS).

Fig. 1 shows the grain morphologies of the three samples. As the Mg-3%Al alloy, its grains are coarse with average size of $715 \pm 55 \mu\text{m}$ (Fig. 1a). After being inoculated by carbon, its grain size was refined to

$205 \pm 15 \mu\text{m}$ (Fig. 1b). The grain size could be further refined to $117 \pm 10 \mu\text{m}$ for the carbon-inoculated Mg-3%Al alloy combining with 0.2% Ca addition (Fig. 1c). The results indicate that Ca addition could promote the refining effect of Mg–Al alloys with carbon inoculation. Fig. 2 illustrates the EPMA-WDS map analysis results of the Al-C-rich nucleating particles and their elements distributions of Al, C, Ca and O. The black particles existed in Fig. 2(a) are Al-C-rich compound (denoted by arrows). The content of Ca is high and it is always overlapped with Al and C for most of the Al-C-rich particles (denoted by arrows) from the Fig. 2(b), (c) and (d). The addition content of Ca is 0.2 wt% in our experiment, while the solubility of Ca in Mg is 0.44 at.% under room temperature. According to Fig. 2(e), the distribution of O elements is almost overlapped with Al, C and Ca. It is well known that the Al-C-O particles (which are originally Al_4C_3 particles) were easily to observe in the Mg–Al based alloys inoculated by carbon, for the Al_4C_3 were easily hydrolyzed during sample preparation resulted from the reaction $\text{Al}_4\text{C}_3(\text{s}) + 12\text{H}_2\text{O}(\text{l}) = 4\text{Al}(\text{OH})_3(\text{s}) + \text{CH}_4(\text{g}) \uparrow$ [39–41]. According to Fig. 2(b), (c) and (d), the distribution of Ca is around the Al–C particles, implying that Ca atoms are adsorbed on the surface of Al_4C_3 particles.

3. Adsorption simulation

It is very difficult to disclose the influence of Ca adsorption on the surface of Al_4C_3 nuclei since analysis cannot be performed at the atomic scale due to limitations of experimental equipment and methods. Coupled with the experimental results, the first-principles calculation was used to study the influence of Ca adsorption on Al_4C_3 surface in the present study. The simulation methods can be used to analyze from the electronic level, where first-principles calculation is an important and effective analysis method [13].

Several adsorption configurations were calculated by the VASP (Vienna ab initio simulation package) code [42], with PAW (projected augmented wave) pseudopotentials [43], and the plane-wave cutoff energy of 340 eV. The GGA (generalized gradient approximation) with the PBE (Perdew-Burke-Ernzerhof) functional [44] was opted as the exchange-correlation functional. The structures were fully relaxed until the forces on each atom were $< 0.01 \text{ eV}/\text{\AA}$. The Brillouin zone was sampled with a uniform $9 \times 9 \times 6$ mesh for the bulk calculation of Al_4C_3 . The adopted Al_4C_3 -slab was a $2 \times 2 \times 1$ supercell, with a corresponding Brillouin zone sampling of a $4 \times 4 \times 1$ mesh for clean surface and adsorption calculations, where the vacuum thickness was set to 20 Å.

3.1. $\text{Al}_4\text{C}_3(0001)$ surfaces

The structural space group of Al_4C_3 is R-3m (No. 166), and the experimental lattice parameters of Al_4C_3 are $a = b = 3.335 \text{ \AA}$ and $c = 24.967 \text{ \AA}$ [45]. The optimized lattice parameters are $a = b = 3.333 \text{ \AA}$ and $c = 24.956 \text{ \AA}$, which are in line with the experimental parameters above. As shown in Fig. 3, the surface configuration of Al_4C_3 is divided into Al-terminated and C-terminated surfaces along c axis. The Al-terminated surface is divided into four types according to

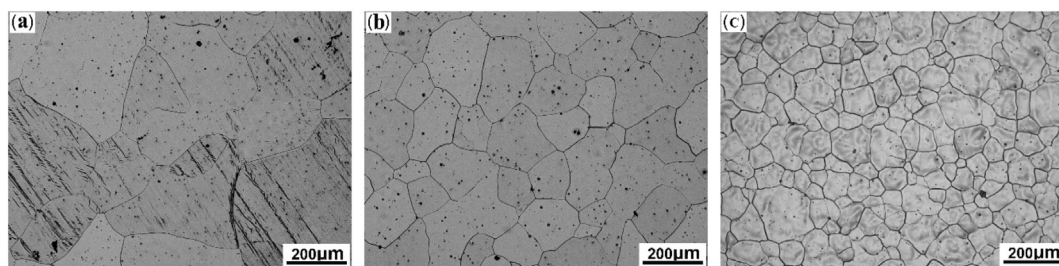


Fig. 1. Optical micrographs showing the effect of an addition of 0.2% Ca into Mg–3Al alloy with carbon inoculation ((a) Mg-3%Al alloy; (b) 0.2 wt.% C addition; (c) 0.2 wt.% C + 0.2 wt.% Ca addition). The holding time of the samples was 30 min.

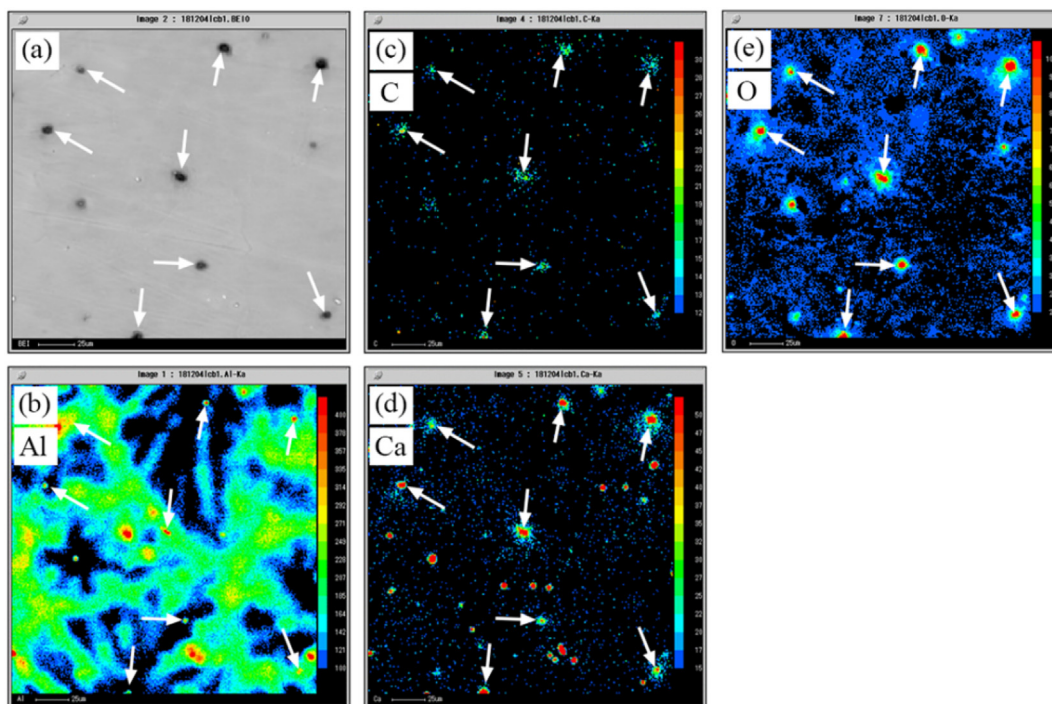


Fig. 2. EPMA-WDS map of the sample refined by carbon inoculation combining Ca addition. (a) The region of EPMA-WDS map analysis; (b)–(e) the distribution of Al, C, Ca and O element, respectively.

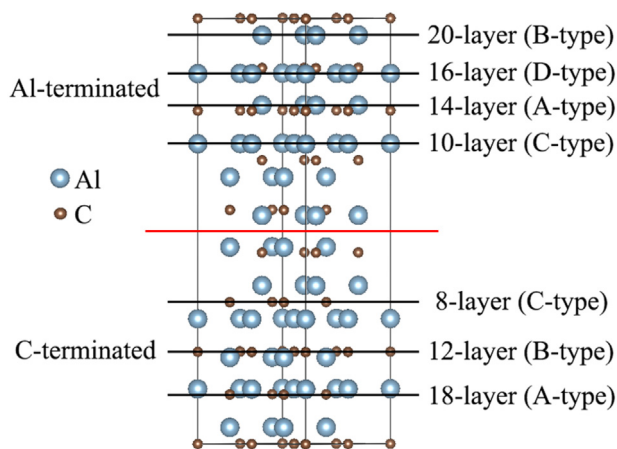


Fig. 3. The $2 \times 2 \times 1$ supercell of bulk Al_4C_3 (the surface configurations are divided into Al-terminated and C-terminated surfaces).

different scenarios: A-type, B-type, C-type and D-type. The A-type surface, i.e., the surface Al atoms are very close to the C atoms of the second layer and they are almost on the same layer. In the B-type surface slab, as shown in Fig. 3, there exists a large distance between the surface-Al atoms and the second-layer-C atoms. The distance between surface-Al atoms and second-layer-C atoms of the C-type is larger than that of A-type and lower than that of B-type. Both the surface layer and the second layer are Al atoms in the D-type. The C-terminated surface is divided into A-type, B-type and C-type surfaces. Their classifications are similar to those of Al-terminated surface. The convergences of different slabs with different number of layers were calculated to select a suitable surface configuration. In the calculation, the middle layers of the slab were fixed and the first six layers of each side were relaxed. The lower the surface energy is, the more stable the slab is. The surface energy of $\text{Al}_4\text{C}_3(0001)$ slab can be given by [20]:

$$\begin{aligned} \sigma_{\text{Al}_4\text{C}_3(0001)} &= \frac{1}{2A} \left[E_{\text{slab}} - \frac{1}{3} N_{\text{C}} \mu_{\text{Al}_4\text{C}_3}^{\text{bulk}} + \left(\frac{4}{3} N_{\text{C}} - N_{\text{Al}} \right) \Delta \mu_{\text{Al}} + \left(\frac{4}{3} N_{\text{C}} - N_{\text{Al}} \right) \mu_{\text{Al}}^{\text{bulk}} \right] \end{aligned} \quad (1)$$

which is derived from the following formulas:

$$\sigma_{\text{Al}_4\text{C}_3(0001)} = \frac{1}{2A} [E_{\text{slab}} - N_{\text{Al}} \mu_{\text{Al}}^{\text{slab}} - N_{\text{C}} \mu_{\text{C}}^{\text{slab}} + PV - TS] \quad (2)$$

$$\mu_{\text{Al}_4\text{C}_3}^{\text{bulk}} = 4\mu_{\text{Al}}^{\text{slab}} + 3\mu_{\text{C}}^{\text{slab}} \quad (3)$$

$$\mu_{\text{Al}_4\text{C}_3}^{\text{bulk}} = 4\mu_{\text{Al}}^{\text{bulk}} + 3\mu_{\text{C}}^{\text{bulk}} + \Delta H_f^0 \quad (4)$$

$$\Delta \mu_{\text{Al}} = \mu_{\text{Al}}^{\text{slab}} - \mu_{\text{Al}}^{\text{bulk}} \quad (5)$$

From the formulas (3) and (4), the range of the Al chemical potential can be given by:

$$\frac{1}{4} \Delta H_f^0 \leq \Delta \mu_{\text{Al}} \leq 0 \quad (6)$$

where A is the surface area of the slab; E_{slab} is the total energy of calculated slab; μ_i^{bulk} is the chemical potential of i -bulk (i represents Al_4C_3 , Al and C); N_{Al} and N_{C} are the number of Al atoms and C atoms of the slab, respectively; μ_i^{slab} is the chemical potential of i atom in the $\text{Al}_4\text{C}_3(0001)$ slab (i represents Al and C); the PV and TS terms may be neglected at the level of 0 K and typical pressures; ΔH_f^0 is the formation enthalpy of Al_4C_3 -bulk at 0 K, and the corresponding calculated value is -0.665 eV.

The calculated surface energies of the optimized Al_4C_3 surface slabs are listed in Table 1. It is clear that the surface energies of the same types of Al-terminated (or C-terminated) surfaces are well converged, but they are remarkably different from each other for the various types of surfaces. According to Fig. 4(a) and (b), we find that the surface energy of A-type 28-layer slab is the lowest. When the A-type of C-terminated slab was relaxed, the first layer of C atoms was migrated into the second layer, and the C-terminated slab is changed to an Al-terminated slab, implying that the A-type slab of C-terminated is

Table 1
The surface energies of the optimized Al₄C₃ surface slabs.

σ (J/m ²) (Al-terminated surfaces)				
$\Delta\mu_{Al}$ (eV)	10-layer (C-type)	14-layer (A-type)	16-layer (D-type)	20-layer (B-type)
-0.166	2.605	1.022	2.198	1.936
0	2.513	1.022	1.922	1.751
$\Delta\mu_{Al}$ (eV)	24-layer (C-type)	28-layer (A-type)	30-layer (D-type)	34-layer (B-type)
-0.166	2.618	1.024	2.198	1.933
0	2.526	1.024	1.922	1.749

σ (J/m ²) (C-terminated surfaces)			
$\Delta\mu_{Al}$ (eV)	8-layer (C-type)	12-layer (B-type)	18-layer (A-type)
-0.166	4.947	10.412	3.160
0	5.132	10.689	3.252
$\Delta\mu_{Al}$ (eV)	22-layer (C-type)	26-layer (B-type)	32-layer (A-type)
-0.166	5.116	10.414	3.157
0	5.301	10.691	3.249
$\Delta\mu_{Al}$ (eV)	36-layer (C-type)		
-0.166	5.116		
0	5.301		

unstable. Based on the calculated surface energies of C-terminated slabs, the 26-layer slab of B-type and the 22-layer slab of C-type are well converged too. It can be seen that the surface energy of 22-layer slab of C-type is lower than that of 26-layer slab of B-type from the Fig. 4(b). However, all the surface energies of C-terminated slabs are higher than those of corresponding Al-terminated slabs. Therefore, the Al₄C₃ structure tends to form Al-terminated surfaces. In addition, the analysis of the percentage change of the interlayer spacing after optimization shows that the structure of the Al-terminated surface slabs is also well converged, as shown in Fig. 5. The surface energy of 28-layer slab (A-type) of the Al-terminated Al₄C₃(0001) is the lowest, and thus it is selected for further investigation of the Al₄C₃(0001) surface.

3.2. Single Ca or Mg adsorption on Al₄C₃(0001) surface

The Ca atoms in the Mg melt are adsorbed and segregated on the

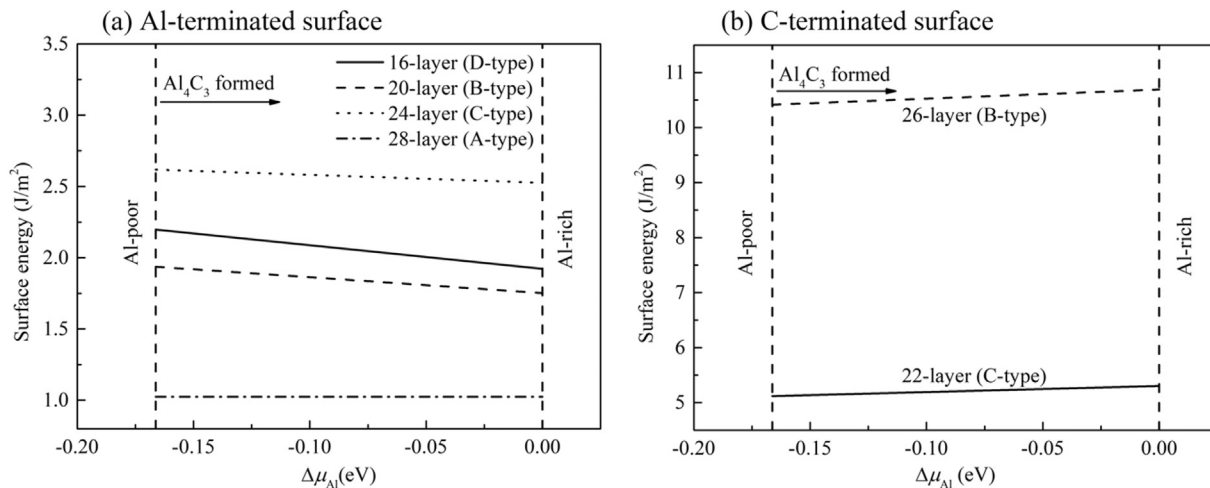


Fig. 4. The surface energies of (a) Al-terminated surface slabs and (b) C-terminated surface slabs.

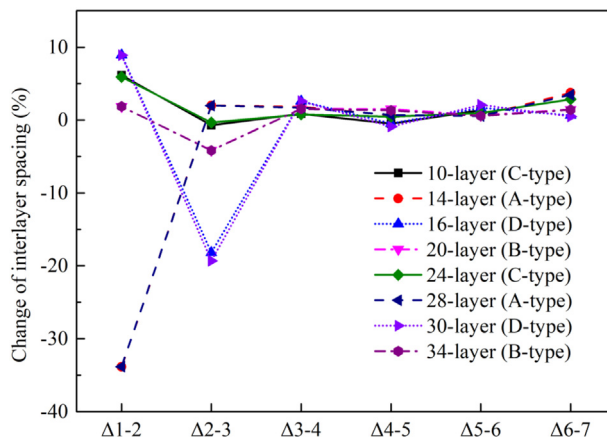


Fig. 5. The percentage change of the interlayer spacing of the relaxed Al-terminated surface slabs.

Al₄C₃ surface as the temperature decreases to the actual crystallization temperature. Meanwhile, the Mg atoms are also adsorbed and grown on the surfaces of Al₄C₃ particles. The adsorption process is critical to determine the heterogeneous nucleation refinement of Al₄C₃ particles, giving insights of the initial process of nucleation. It is helpful to study the adsorption of Ca and Mg on the Al₄C₃(0001) surface in order to judge the influence of the presence of Ca on the grain refinement of Al₄C₃ heterogeneous nucleation. In the adsorption calculation, the 28-layer slab (A-type) of Al-terminated Al₄C₃(0001) surface was used to simulate the surface. We have calculated the high symmetry adsorption sites for Ca or Mg atom on Al₄C₃(0001) surface, including H1, H2, T and B sites. The results of B (bridge site) are not shown in Fig. 6(a) as it turns out to be unstable, while the results of H1, H2 and T sites are shown. We considered four slabs with adsorption coverage of 0.25 ML, 0.5 ML, 0.75 ML and 1 ML, respectively. The adsorption concentration is the ratio of the number of adsorbed atoms on the surface to the number of atoms in the surface layer. The adsorption energies of single Ca or Mg adsorption on Al₄C₃(0001) surface can be given by:

$$E_{ad} = [(E_{Al_4C_3(0001)} + n_i E_i) - E_{i/Al_4C_3(0001)}] / n_i \tag{7}$$

here $E_{Al_4C_3(0001)}$ is the energy of Al-terminated Al₄C₃ (0001) clean surface; n_i is the number of adsorption Ca or Mg atoms, respectively; E_i is the energy of a single Ca or Mg atom, with i corresponds to atom Ca or Mg accordingly; $E_{i/Al_4C_3(0001)}$ is the total energy of the Al-terminated Al₄C₃(0001) slab with Ca or Mg adsorbed. Positive adsorption energies stand for the energetically favored cases.

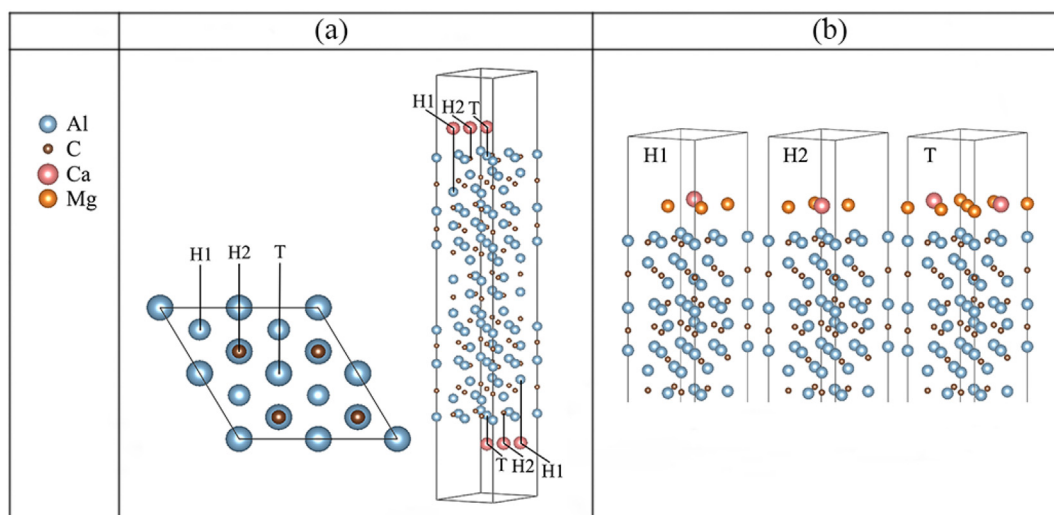


Fig. 6. Adsorption diagram (a) The schematic diagram of adsorption sites that Ca or Mg adsorption on the 28-layer (A-type) of Al-terminated Al₄C₃(0001) surface (taking the adsorption sites with Ca atoms for illustration) (b) the schematic diagram of adsorption sites that Ca and Mg co-adsorption on the 28-layer (A-type) of Al-terminated Al₄C₃(0001) surface.

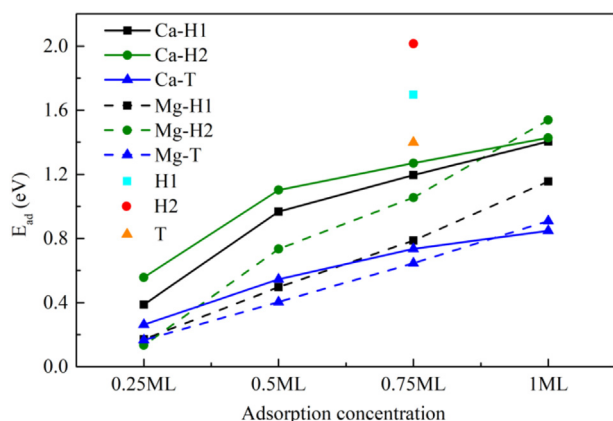


Fig. 7. The adsorption energies of Ca or Mg adsorption on Al-terminated Al₄C₃(0001) surface. The solid and dashed lines represent the adsorption energy of single Ca and Mg on the Al₄C₃(0001) surface, respectively. The discrete points represent the adsorption energy of Mg when co-adsorbed with Ca atom.

The calculated adsorption energies are shown in Fig. 7, showing that Ca tends to be adsorbed at the H2 site of Al-terminated Al₄C₃(0001) surface as it has the greatest adsorption energy in general. From 0.25 ML to 1 ML, the adsorption energies become greater as the coverage increases since the additional Ca atoms interact with both the surface Al atoms and the earlier adsorbed Ca atoms. Interestingly, the adsorption energies of Mg at 0.25 ML coverage has no remarkable difference at H1, H2 and T sites on Al₄C₃(0001) surface, as shown in Fig. 7. When the coverage increases, Mg prefers to the H2 site. In the Mg melt, the Al₄C₃ particles are surrounded by Mg melt environment and a large amount of Mg atoms are supplied, therefore, the Mg atoms tend to accumulate at the H2 sites under experimental condition. Comparing the adsorption energies of Ca and Mg atoms adsorption on the Al₄C₃ surface, the adsorption energies of Ca are greater than that of Mg at the same adsorption site in general. It indicates that Ca atoms are easier adsorbed on the Al₄C₃ surface than the Mg atoms. This explains the experimental observation of Ca adsorption around the Al–C phase.

3.3. Co-adsorption of Ca and Mg atoms on Al₄C₃(0001) surface

According to the above discussion, we revealed that Ca atoms are easier to adsorb on the Al₄C₃ surface with respect to Mg atoms. Here,

we continue to study the influence of Ca on the Mg adsorption on Al₄C₃(0001) surface. Since the amount of Ca was not great (0.2 wt% Ca) while Mg atoms can be continuously supplied in the Mg melt, we calculated the E_{ad} of single Ca adsorption on Al₄C₃(0001) surface at 1/4 ML and 1/8 ML coverages, respectively. The E_{ad} of Ca is 0.557 eV at 1/4 ML and it can be applied to the diluted case as it changes little to the 1/8 ML case, 0.534 eV. Therefore, the adsorption configuration of 1:3 for Ca and Mg is considered in our $2 \times 2 \times 1$ surface model. Three adsorption sites were considered, including: H1, H2 and T sites, as shown in Fig. 6(b).

The adsorption energies of Mg adsorption on a Ca pre-adsorbed Al₄C₃(0001) surface can be given by:

$$E_{ad} = [E_{Ca/Al_4C_3(0001)} + n_{Mg}E_{Mg} - E_{(Ca+Mg)/Al_4C_3(0001)}]/n_{Mg} \quad (8)$$

E_{ad} is the adsorption energy of Mg adsorption on Al₄C₃(0001) surface; $E_{Ca/Al_4C_3(0001)}$ is the total energy of the slab that one Ca atom adsorption on Al₄C₃(0001) surface; n_{Mg} is the number of adsorbed Mg atoms; E_{Mg} is the energy of single Mg atom; $E_{(Ca+Mg)/Al_4C_3(0001)}$ is the total energy of the slab that one Ca atom and three Mg atoms co-adsorption on Al₄C₃(0001) surface.

The calculated adsorption energies are shown in Fig. 7, indicating that the adsorption energy of Mg increases on the Ca pre-adsorbed surface, much greater than that on clean Al₄C₃ surfaces. It means that the presence of Ca promotes the adsorption of Mg atoms on Al₄C₃(0001) surface, and more Al₄C₃ particles can act as heterogeneous nucleation refiner. This explains why the grain size of 0.2 wt.% C + 0.2 wt.% Ca experimental group (shown in Fig. 1c) is smaller than that of 0.2 wt.% C experimental group (see Fig. 1b).

3.4. Electronic structure and further discussions

The calculated DOS of Al₄C₃-bulk is shown in Fig. 8, indicating that the bulk Al₄C₃ is a semiconductor with a band gap of 1.32 eV. The surface layer becomes metallic when adsorbed with the relative high coverage of Ca and Mg atoms, as the gap disappear in the calculated DOS of adsorbed systems (see Fig. 9). According to Fig. 9(a) and (b), the projected DOSs (PDOS) of surface Al and C atoms are significantly different in various adsorbed slabs, indicating that the adsorbed atoms have strong interactions with the surface atoms. The presence of Ca atom also has a great influence on the Mg atom, as there are remarkable difference between the PDOS of Mg atoms in the cases of single Mg adsorption and co-adsorption with Ca (cf. Fig. 9c). In Fig. 9(d), the

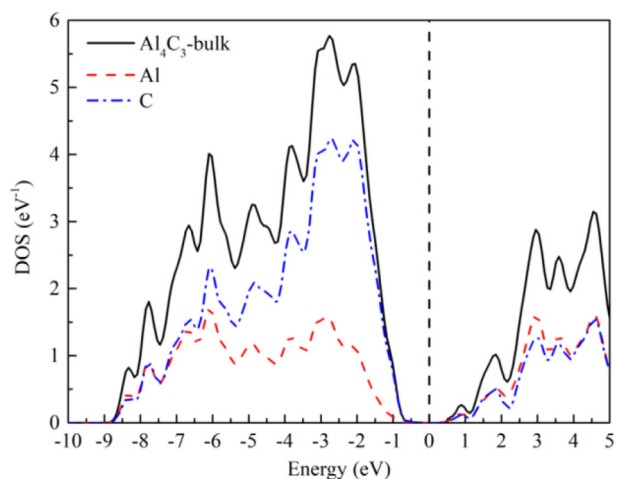


Fig. 8. Density of states (DOS) of Al_4C_3 -bulk and corresponding projected DOSs of Al and C atoms.

single PDOS peaks of Ca atom (both single and co-adsorbed) ranged above the Fermi level, indicating the ionic characteristic of Ca on Al_4C_3 surface.

As the PDOS of different atoms in the slab that Ca and Mg co-adsorption on Al_4C_3 surface shown in Fig. 9, the surface-Al atoms and the surface-C atoms resonate at a peak between -6.5 eV and -5 eV and between -3 eV and -1 eV. The DOS curve of adsorbed Ca atom and adsorbed Mg atom resonate at a peak between -1.5 eV and 5 eV. The

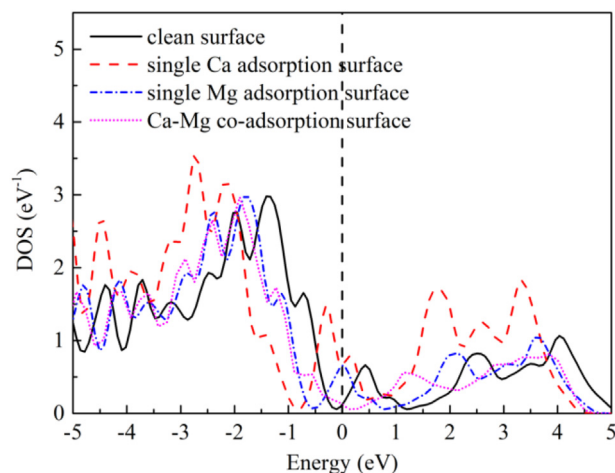


Fig. 10. Density of states of $\text{Al}_4\text{C}_3(0001)$ surface for (a) $\text{Al}_4\text{C}_3(0001)$ clean surface, (b) single Ca adsorbed $\text{Al}_4\text{C}_3(0001)$ surface, (c) single Mg adsorbed $\text{Al}_4\text{C}_3(0001)$ surface, (d) Ca and Mg co-adsorbed $\text{Al}_4\text{C}_3(0001)$ surface.

adsorbed Ca, adsorbed Mg, surface-Al and surface-C all resonate at peaks around 0.5 eV– 2 eV and 2 eV– 5 eV. The above calculated results indicate that these atoms form bonds with each other. The calculated DOSs of $\text{Al}_4\text{C}_3(0001)$ slab in different models are shown in Fig. 10. It shows that peaks of adsorbed models shift towards the lower energy in contrast to clean model, especially the single Ca adsorbed Al_4C_3 surface. This indicates that the adsorbed surfaces are more stable than Al_4C_3 clean surface, and the Al_4C_3 surface of single Ca adsorbed model is the

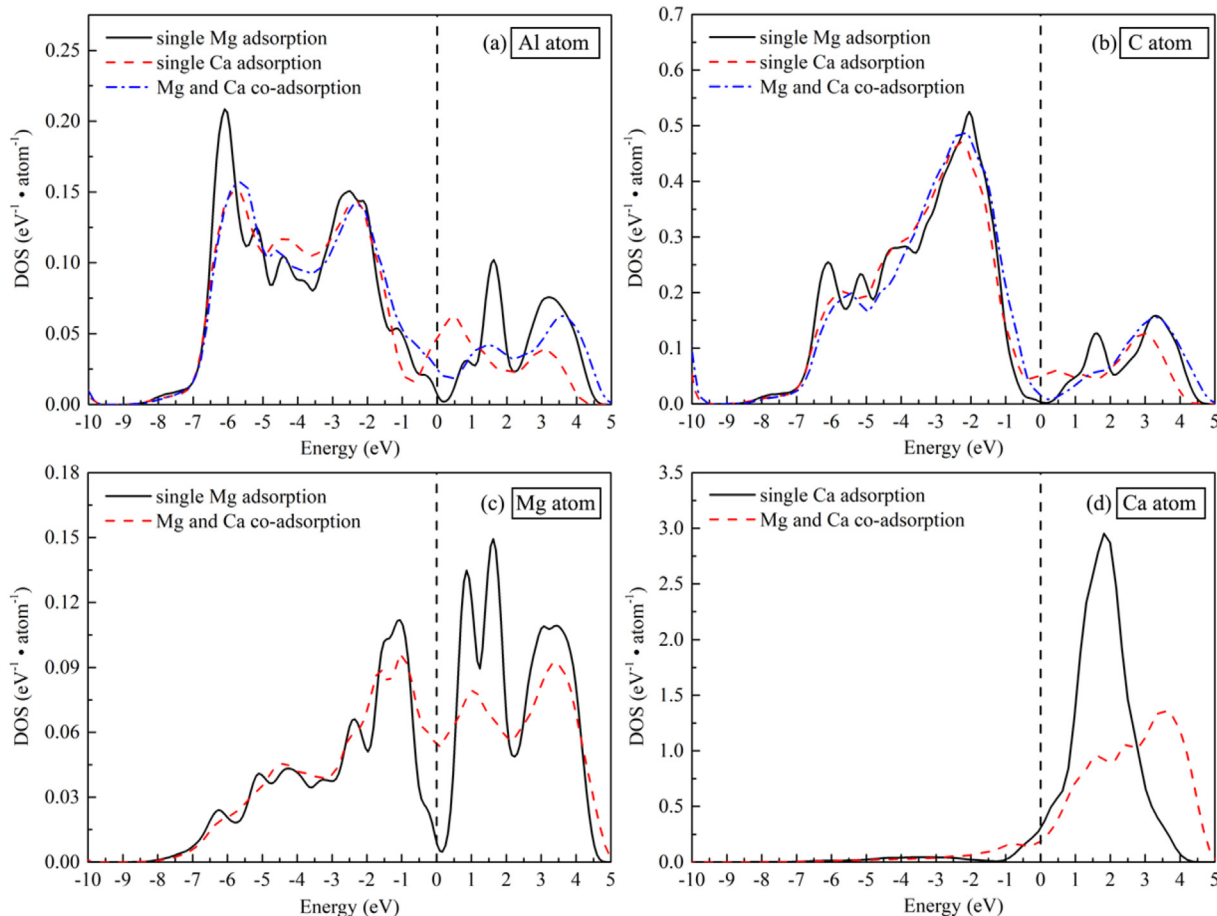


Fig. 9. Projected density of states (PDOS) for (a) The surface Al atom, (b) the surface C atom, (c) the adsorbed Mg atom, (d) the adsorbed Ca atom in various situations.

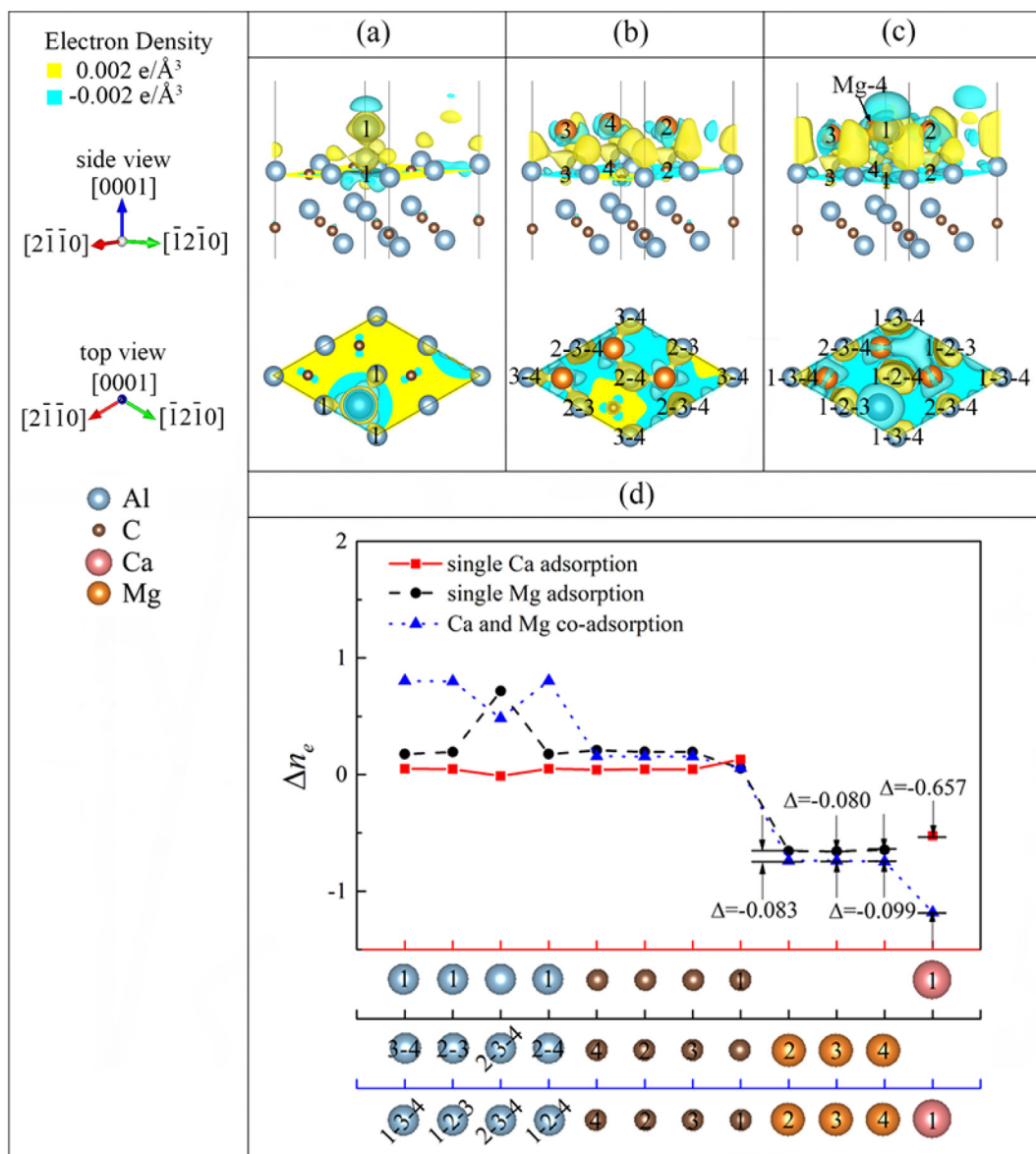


Fig. 11. The charge density difference before and after adsorption for the $\text{Al}_4\text{C}_3(0001)$ slabs with (a) single Ca adsorbed, (b) single Mg adsorbed, and (c) Mg–Ca co-adsorbed, as well as (d) the Bader charge of chosen atoms in these systems, represented by red, black and blue, respectively. The numbers labeled on the atoms in (d) plot indicates its nearest neighbor atoms as shown in (a), (b) and (c) plots.

most stable.

From Fig. 11(a), (b) and (c), we see that the adsorbed Ca atom and adsorbed Mg atoms lose charges, while the surface-Al atoms and surface-C atoms gain charges. An ionic bond is formed between the adsorbed Ca atom and the surface-C atom as there is a significant charge separation between them, in line with the ionic characteristic of Ca according to the PDOS of Ca in Fig. 9(d). A mixed ionic/covalent bond is formed between the adsorbed Mg atom and the surface-C atom for the charge accumulation exists between them. According to the Fig. 11(d), the charge of the surface-Al atom and the surface-C atom in the adsorption slab is more than those in the clean Al_4C_3 surface slab, respectively. At the presence of Ca, the charges of the three adsorbed Mg atoms lose 0.083e, 0.080e, and 0.099e more than those without Ca, respectively. Interestingly, the Ca atom loses 0.657e more when co-adsorbed with Mg than its single adsorption case. Nevertheless, the additional of Ca atoms further stabilizes the Mg adsorbed Al_4C_3 slabs.

According to the calculated results above, the adsorption energies of Ca are greater than that of Mg at the same adsorption site in general. The adsorption energy of Mg increases remarkably when it co-adsorbed

with Ca, with respect to the single Mg adsorption case on Al_4C_3 surface. Ca atoms are easier adsorbed on the Al_4C_3 surface than Mg atoms, and the presence of Ca atoms promotes the adsorption of Mg on the Al_4C_3 surface. A comprehensive analysis of the calculated results explains that why the refinement effect of the 0.2 wt.% C + 0.2 wt.% Ca experimental group is better than that of the 0.2 wt.% C experimental group. Combing all the calculated results above, the presence of Ca changed the structure, the electronic structure and bonding of Al_4C_3 surfaces. These changes promote the potential of Al_4C_3 particles acting as stable heterogeneous nucleus and thus refine the primary Mg grains subsequently.

4. Conclusions

In this paper, we studied the influence of Ca on the heterogeneous nucleation of Al_4C_3 particles by experimental and computational method. Summarized as follows:

1. The refinement effect of the 0.2 wt.% C + 0.2 wt.% Ca experiment is

better than that of the 0.2 wt.% C experiment. The results of EPMA experiment show that Ca adsorbs around the Al–C phase.

- Both Ca and Mg atoms tend to adsorb at the H2 site of the Al-terminated $Al_4C_3(0001)$ surface, which is demonstrated as the most stable surface with surface energy of 1.024 J/m^2 . Besides, the adsorption energy of Mg atom increases significantly at the presence of Ca atom, indicating that Ca atom promotes the adsorption of Mg on the Al-terminated $Al_4C_3(0001)$ surface.
- Based on the calculated results, the Ca atoms are apt to adsorb on the Al_4C_3 surface and promote heterogeneous nucleating effect of Al_4C_3 . The adsorption slab is more stable and more Al_4C_3 particles can function as a stable heterogeneous nucleation at the presence of Ca atom. The element Ca and Al_4C_3 particles play a synergistic role on the grain refinement of the magnesium alloys.

Acknowledgments

This work was supported by the National Natural Science Foundation of China (51574127, 11574088) and Natural Science Foundation of Guangdong Province (2014A030313221).

References

- A.A. Luo, Magnesium casting technology for structural applications, *J. Magn. Alloys* 1 (2013) 2–22.
- X.J. Wang, D.K. Xu, R.Z. Wu, X.B. Chen, Q.M. Peng, L. Jin, Y.C. Xin, Z.Q. Zhang, Y. Liu, X.H. Chen, G. Chen, K.K. Deng, H.Y. Wang, What is going on in magnesium alloys? *J. Mater. Sci. Technol.* 34 (2017) 245–247.
- Y. Ali, D. Qiu, B. Jiang, F.S. Pan, M.X. Zhang, Current research progress in grain refinement of cast magnesium alloys: a review article, *J. Alloys Compd.* 619 (2015) 639–651.
- M.A. Easton, M. Qian, A. Prasad, D.H. StJohn, Recent advances in grain refinement of light metals and alloys, *Curr. Opin. Solid State Mater. Sci.* 20 (2016) 13–24.
- H.H. Yu, Y.C. Xin, M.Y. Wang, Q. Liu, Hall-Petch relationship in Mg alloys: a review, *J. Mater. Sci. Technol.* 34 (2018) 248–256.
- M. Qian, P. Cao, Discussions on grain refinement of magnesium alloys by carbon inoculation, *Scr. Mater.* 52 (2005) 415–419.
- S.F. Liu, Y. Chen, H. Han, Grain refinement of AZ91D magnesium alloy by a new Mg-50% Al_4C_3 master alloy, *J. Alloys Compd.* 624 (2015) 266–269.
- Q.L. Jin, J.P. Eom, S.G. Lim, W.W. Park, B.S. You, Reply to comments on “Grain refining mechanism of a carbon addition method in a Mg–Al magnesium alloy”, *Scr. Mater.* 52 (2005) 421–423.
- M.X. Han, X.Z. Zhu, T. Gao, X.F. Liu, Revealing the roles of Al_4C_3 and Al_6Mn_5 during α -Mg nucleation in Mg–Al based alloys, *J. Alloys Compd.* 705 (2017) 14–21.
- D. Turnbull, B. Vonnegut, Nucleation catalysis, *Ind. Eng. Chem.* 44 (1952) 1292–1298.
- B.L. Bramfitt, The effect of carbide and nitride additions on the heterogeneous nucleation behavior of liquid iron, *Metall. Trans.* 1 (1970) 1987–1995.
- M.X. Zhang, P.M. Kelly, Crystallography and morphology of widmanstätten cementite in austenite, *Acta Mater.* 46 (1998) 4617–4628.
- D.W. Shin, C. Wolverton, First-principles density functional calculations for Mg alloys: a tool to aid in alloy development, *Scr. Mater.* 63 (2010) 680–685.
- F. Wang, K. Li, N.G. Zhou, First-principles calculations on Mg/ Al_2O_3 interfaces, *Appl. Surf. Sci.* 285 (2013) 879–884.
- N.R. D’Amico, G. Cantele, C.A. Perroni, D. Ninno, Electronic properties and Schottky barriers at ZnO-metal interfaces from first principles, *J. Phys. Condens. Matter.* 27, 2015, Article 015006.
- J. Yang, J.H. Huang, D.Y. Fan, S.H. Chen, X.K. Zhao, $LaAlO_3$ as the heterogeneous nucleus of ferrite: experimental investigation and theoretical calculation, *J. Alloys Compd.* 683 (2016) 357–369.
- J.X. Yang, L. Chen, J.L. Fan, H.R. Gong, Doping of helium at Fe/W interfaces from first principles calculation, *J. Alloys Compd.* 686 (2016) 160–167.
- J. Li, M. Zhang, Y. Zhou, G.X. Chen, First-principles study of Al/ Al_3Ti heterogeneous nucleation interface, *Appl. Surf. Sci.* 307 (2014) 593–600.
- Z. Fan, Y. Wang, Y. Zhang, T. Qin, X.R. Zhou, G.E. Thompson, T. Pennycook, T. Hashimoto, Grain refining mechanism in the Al/Al–Ti–B system, *Acta Mater.* 84 (2015) 292–304.
- K. Li, Z.G. Sun, F. Wang, N.G. Zhou, X.W. Hu, First-principles calculations on Mg/ Al_4C_3 interfaces, *Appl. Surf. Sci.* 270 (2013) 584–589.
- H.L. Wang, J.J. Tang, Y.J. Zhao, J. Du, First-principles study of Mg/ Al_2MgC_2 heterogeneous nucleation interfaces, *Appl. Surf. Sci.* 355 (2015) 1091–1097.
- W.W. Xu, A.P. Horsfield, D. Wearing, P.D. Lee, First-principles calculation of Mg/MgO interfacial free energies, *J. Alloys Compd.* 650 (2015) 228–238.
- J. Du, H.L. Wang, M.C. Zhou, W.F. Li, Poisoning-free effect of calcium on grain refinement of Mg-3%Al alloy containing trace Fe by carbon inoculation, *Trans. Nonferrous Metals Soc. China* 23 (2013) 307–314.
- H. Men, Z. Fan, Effects of solute content on grain refinement in an isothermal melt, *Acta Mater.* 59 (2011) 2704–2712.
- J. Du, M.H. Wang, W.F. Li, Effects of Fe addition and addition sequence on carbon inoculation of Mg-3%Al alloy, *J. Alloys Compd.* 502 (2010) 74–79.
- J. Du, J. Yang, M. Kuwabara, W.F. Li, J.H. Peng, Effect of strontium on the grain refining efficiency of Mg-3Al alloy refined by carbon inoculation, *J. Alloys Compd.* 470 (2009) 228–232.
- J. Du, J. Yang, M. Kuwabara, W.F. Li, J.H. Peng, Effects of manganese and/or carbon on the grain refinement of Mg-3Al alloy, *Mater. Trans.* 49 (2008) 139–143.
- J. Du, J. Yang, M. Kuwabara, W.F. Li, J.H. Peng, Effect of iron and/or carbon on the grain refinement of Mg-3Al alloy, *Mater. Trans.* 48 (2007) 2903–2908.
- P. Cao, M. Qian, D.H. StJohn, Effect of manganese on grain refinement of Mg–Al based alloys, *Scr. Mater.* 54 (2006) 1853–1858.
- Y.C. Lee, A.K. Dahle, D.H. StJohn, The role of solute in grain refinement of magnesium, *Metall. Mater. Trans. A* 31A (2000) 2895–2906.
- L.F. Yao, K. Li, N.G. Zhou, First-principles study of Mn adsorption on $Al_4C_3(0001)$ surface, *Appl. Surf. Sci.* 363 (2016) 168–172.
- C.H. Wei, K. Li, L.F. Yao, N.G. Zhou, Influence of Fe on Al_4C_3 as a heterogeneous nucleation substrate: a first-principles study, *Mater. Res. Express* 4 (2017) 106517.
- W.T. Kim, B. Cantor, An adsorption model of the heterogeneous nucleation of solidification, *Acta Metall. Mater.* 42 (1994) 3115–3127.
- B. Cantor, Heterogeneous nucleation and adsorption, *Philos. Trans. R. Soc. Lond. A* 361 (2003) 409–417.
- J. Du, J. Yang, M. Kuwabara, W.F. Li, J.H. Peng, Improvement of grain refining efficiency for Mg–Al alloy modified by the combination of carbon and calcium, *J. Alloys Compd.* 470 (2009) 134–140.
- S.S. Li, B. Tang, D.B. Zeng, Effects and mechanism of Ca on refinement of AZ91D alloy, *J. Alloys Compd.* 437 (2007) 317–321.
- B. Nagasivamuni, K.R. Ravi, An analytical approach to elucidate the mechanism of grain refinement in calcium added Mg–Al alloys, *J. Alloys Compd.* 622 (2015) 789–795.
- C.B. Li, C. Wen, J. Du, W.F. Li, M.Y. Zhan, Inoculant fading-resistance of Fe-bearing Mg-3%Al alloys refined by carbon combining with calcium, addition, *Mater. Trans.* 59 (2018) 1878–1886.
- L. Lu, A.K. Dahle, D.H. StJohn, Grain refinement efficiency and mechanism of aluminium carbide in Mg–Al alloys, *Scr. Mater.* 53 (2005) 517–522.
- P. Cao, M. Qian, D.H. StJohn, Mechanism for grain refinement of magnesium alloys by superheating, *Scr. Mater.* 56 (2007) 633–636.
- J. Du, Y.T. Shi, M.C. Zhou, W.F. Li, Effect of Sr on grain refinement of Mg-3%Al alloy containing trace Fe by carbon-inoculation, *J. Mater. Sci. Technol.* 32 (2016) 1297–1302.
- G. Kresse, J. Furthmüller, Efficient iterative schemes for *ab initio* total-energy calculations using a plane-wave basis set, *Phys. Rev. B* 54 (1996) 11169–11186.
- P.E. Blöchl, Projector augmented-wave method, *Phys. Rev. B* 50 (1994) 17953–17979.
- J.A. White, D.M. Bird, Implementation of gradient-corrected exchange-correlation potentials in Car-Parrinello total-energy calculations, *Phys. Rev. B* 50 (1994) 4954–4957.
- T.M. Gesing, W. Jeitschko, The crystal structure and chemical properties of $U_2Al_3C_4$ and structure refinement of Al_4C_3 , *Z. Naturforsch.* 50b (1995) 196–200.